MIT Open Access Articles

Measurement of branching fractions and rate asymmetries in the rare decays B→K [superscript (*)]#[superscript +]#[superscript -]

Massachusetts Institute of Technology

Measurement of branching fractions and rate asymmetries in the rare decays $B \to K^{(*)}\ell^+\ell^-$

J. P. Lees,[1] V. Poireau,[1] V. Tisserand,[1] J. Garra Tico,[2] E. Grauges,[2] A. Palano,[3a,3b] G. Eigen,[4] B. Stugu,[4] D. N. Brown,[5] L. T. Kerth,[5] Yu. G. Kolomensky,[5] G. Lynch,[5] H. Koch,[6] T. Schroeder,[6] D. J. Asgeirsson,[7] C. Hearty,[7] T. S. Mattison,[7] J. A. McKenna,[7] A. Khan,[8] V. E. Blinov,[9] A. R. Buzykaev,[9] V. P. Druzhinin,[9] V. B. Golubev,[9] E. A. Kravchenko,[9] A. P. Onuchin,[9] S. I. Serednyakov,[9] Yu. I. Skovpen,[9] E. P. Solodov,[9] K. Yu. Todyshev,[9] A. N. Yushkov,[9] M. Bondioli,[10] D. Kirkby,[10] A. J. Lankford,[10] M. Mandelkern,[10] H. Atmacan,[11] J. W. Gary,[11] F. Liu,[11] O. Long,[11] G. M. Vitug,[11] C. Campagnari,[12] T. M. Hong,[12] D. Kovalskyi,[12] J. D. Richman,[12] C. A. West,[12] A. M. Eisner,[13] J. Kroseberg,[13] W. S. Lockman,[13] A. J. Martinez,[13] B. A. Schumm,[13] A. Seiden,[13] D. S. Chao,[14] C. H. Cheng,[14] B. Echenard,[14] K. T. Flood,[14] D. G. Hitlin,[14] P. Ongmongkolkul,[14] F. C. Porter,[14] A. Y. Rakitin,[14] R. Andreassen,[15] Z. Huard,[15] B. T. Meadows,[15] M. D. Sokoloff,[15] L. Sun,[15] P. C. Bloom,[16] W. T. Ford,[16] A. Gaz,[16] U. Nauenberg,[16] J. G. Smith,[16] S. R. Wagner,[16] R. Ayad,[17,*] W. H. Toki,[17] B. Spaan,[18] K. R. Schubert,[19] R. Schwierz,[19] D. Bernard,[20] M. Verderi,[20] P. J. Clark,[21] S. Playfer,[21] D. Bettoni,[22a] C. Bozzi,[22a] R. Calabrese,[22a,22b] G. Cibinetto,[22a,22b] E. Fioravanti,[22a,22b] I. Garzia,[22a,22b] E. Luppi,[22a,22b] M. Munerato,[22a,22b] M. Negrini,[22a,22b] L. Piemontese,[22a] V. Santoro,[22a] R. Baldini-Ferroli,[23] A. Calcaterra,[23] R. de Sangro,[23] G. Finocchiaro,[23] P. Patteri,[23] I. M. Peruzzi,[23,†] M. Piccolo,[23] M. Rama,[23] A. Zallo,[23] R. Contri,[24a,24b] E. Guido,[24a,24b] M. Lo Vetere,[24a,24b] M. R. Monge,[24a,24b] S. Passaggio,[24a] C. Patrignani,[24a,24b] E. Robutti,[24a] B. Bhuyan,[25] V. Prasad,[25] C. L. Lee,[26] M. Morii,[26] A. J. Edwards,[27] A. Adametz,[28] U. Uwer,[28] H. M. Lacker,[29] T. Lueck,[29] P. D. Dauncey,[30] P. K. Behera,[31] U. Mallik,[31] C. Chen,[32] J. Cochran,[32] W. T. Meyer,[32] S. Prell,[32] A. E. Rubin,[32] A. V. Gritsan,[33] Z. J. Guo,[33] N. Arnaud,[34] M. Davier,[34] D. Derkach,[34] G. Grosdidier,[34] F. Le Diberder,[34] A. M. Lutz,[34] B. Malaescu,[34] P. Roudeau,[34] M. H. Schune,[34] A. Stocchi,[34] G. Wormser,[34] D. J. Lange,[35] D. M. Wright,[35] C. A. Chavez,[36] J. P. Coleman,[36] J. R. Fry,[36] E. Gabathuler,[36] D. E. Hutchcroft,[36] D. J. Payne,[36] C. Touramanis,[36] A. J. Bevan,[37] F. Di Lodovico,[37] R. Sacco,[37] M. Sigamani,[37] G. Cowan,[38] D. N. Brown,[39] C. L. Davis,[39] A. G. Denig,[40] M. Fritsch,[40] W. Gradl,[40] K. Griessinger,[40] A. Hafner,[40] E. Prencipe,[40] R. J. Barlow,[41,‡] G. Jackson,[41] G. D. Lafferty,[41] E. Behn,[42] R. Cenci,[42] B. Hamilton,[42] A. Jawahery,[42] D. A. Roberts,[42] C. Dallapiccola,[43] R. Cowan,[44] D. Dujmic,[44] G. Sciolla,[44] R. Cheaib,[45] D. Lindemann,[45] P. M. Patel,[45] S. H. Robertson,[45] P. Biassoni,[46a,46b] N. Neri,[46a] F. Palombo,[46a,46b] S. Stracka,[46a,46a] L. Cremaldi,[47] R. Godang,[47,§] R. Kroeger,[47] P. Sonnek,[47] D. J. Summers,[47] X. Nguyen,[48] M. Simard,[48] P. Taras,[48] G. De Nardo,[49a,49b] D. Monorchio,[49a,49b] G. Onorato,[49a,49b] C. Sciacca,[49a,49b] M. Martinelli,[50] G. Raven,[50] C. P. Jessop,[51] J. M. LoSecco,[51] W. F. Wang,[51] K. Honscheid,[52] R. Kass,[52] J. Brau,[53] R. Frey,[53] N. B. Sinev,[53] D. Strom,[53] E. Torrence,[53] E. Feltresi,[54a,54b] N. Gagliardi,[54a,54b] M. Margoni,[54a,54b] M. Morandin,[54a] M. Posocco,[54a] M. Rotondo,[54a] G. Simi,[54a] F. Simonetto,[54a,54b] R. Stroili,[54a,54b] S. Akar,[55] E. Ben-Haim,[55] M. Bomben,[55] G. R. Bonneaud,[55] H. Briand,[55] G. Calderini,[55] J. Chauveau,[55] O. Hamon,[55] Ph. Leruste,[55] G. Marchiori,[55] J. Ocariz,[55] S. Sitt,[55] M. Biasini,[56a,56b] E. Manoni,[56a,56b] S. Pacetti,[56a,56b] A. Rossi,[56a,56b] C. Angelini,[57a,57b] G. Batignani,[57a,57b] S. Bettarini,[57a,57b] M. Carpinelli,[57a,57b,||] G. Casarosa,[57a,57b] A. Cervelli,[57a,57b] F. Forti,[57a,57b] M. A. Giorgi,[57a,57b] A. Lusiani,[57a,57c] B. Oberhof,[57a,57b] E. Paoloni,[57a,57b] A. Perez,[57a] G. Rizzo,[57a,57b] J. J. Walsh,[57a] D. Lopes Pegna,[58] J. Olsen,[58] A. J. S. Smith,[58] A. V. Telnov,[58] F. Anulli,[59a] R. Faccini,[59a,59b] F. Ferrarotto,[59a] F. Ferroni,[59a,59b] M. Gaspero,[59a,59b] L. Li Gioi,[59a] M. A. Mazzoni,[59a] G. Piredda,[59a] C. Bünger,[60] O. Grünberg,[60] T. Hartmann,[60] T. Leddig,[60] H. Schröder,[60] C. Voss,[60] R. Waldi,[60] T. Adye,[61] E. O. Olaiya,[61] F. F. Wilson,[61] S. Emery,[62] G. Hamel de Monchenault,[62] G. Vasseur,[62] Ch. Yèche,[62] D. Aston,[63] D. J. Bard,[63] R. Bartoldus,[63] J. F. Benitez,[63] C. Cartaro,[63] M. R. Convery,[63] J. Dorfan,[63] G. P. Dubois-Felsmann,[63] W. Dunwoodie,[63] M. Ebert,[63] R. C. Field,[63] M. Franco Sevilla,[63] B. G. Fulsom,[63] A. M. Gabareen,[63] M. T. Graham,[63] P. Grenier,[63] C. Hast,[63] W. R. Innes,[63] M. H. Kelsey,[63] P. Kim,[63] M. L. Kocian,[63] D. W. G. S. Leith,[63] P. Lewis,[63] B. Lindquist,[63] S. Luitz,[63] V. Luth,[63] H. L. Lynch,[63] D. B. MacFarlane,[63] D. R. Muller,[63] H. Neal,[63] S. Nelson,[63] M. Perl,[63] T. Pulliam,[63] B. N. Ratcliff,[63] A. Roodman,[63] A. A. Salnikov,[63] R. H. Schindler,[63] A. Snyder,[63] D. Su,[63] M. K. Sullivan,[63] J. Va'vra,[63] A. P. Wagner,[63] W. J. Wisniewski,[63] M. Wittgen,[63] D. H. Wright,[63] H. W. Wulsin,[63] C. C. Young,[63] V. Ziegler,[63] W. Park,[64] M. V. Purohit,[64] R. M. White,[64] J. R. Wilson,[64] A. Randle-Conde,[65] S. J. Sekula,[65] M. Bellis,[66] P. R. Burchat,[66] T. S. Miyashita,[66] M. S. Alam,[67] J. A. Ernst,[67] R. Gorodeisky,[68] N. Guttman,[68] D. R. Peimer,[68] A. Soffer,[68] P. Lund,[69] S. M. Spanier,[69] J. L. Ritchie,[70] A. M. Ruland,[70] R. F. Schwitters,[70] B. C. Wray,[70] J. M. Izen,[71] X. C. Lou,[71] F. Bianchi,[72a,72b] D. Gamba,[72a,72b] L. Lanceri,[73a,73b] L. Vitale,[73a,73b] F. Martinez-Vidal,[74] A. Oyanguren,[74] H. Ahmed,[75] J. Albert,[75] Sw. Banerjee,[75] F. U. Bernlochner,[75] H. H. F. Choi,[75] G. J. King,[75] R. Kowalewski,[75] M. J. Lewczuk,[75] I. M. Nugent,[75] J. M. Roney,[75] R. J. Sobie,[75] N. Tasneem,[75] T. J. Gershon,[76] P. F. Harrison,[76] T. E. Latham,[76] E. M. T. Puccio,[76] H. R. Band,[77] S. Dasu,[77] Y. Pan,[77] R. Prepost,[77] and S. L. Wu[77]

(*BABAR* Collaboration)

[1]*Laboratoire d'Annecy-le-Vieux de Physique des Particules (LAPP), Université de Savoie, CNRS/IN2P3, F-74941 Annecy-Le-Vieux, France*
[2]*Universitat de Barcelona, Facultat de Fisica, Departament ECM, E-08028 Barcelona, Spain*
[3a]*INFN Sezione di Bari, I-70126 Bari, Italy*
[3b]*Dipartimento di Fisica, Università di Bari, I-70126 Bari, Italy*
[4]*University of Bergen, Institute of Physics, N-5007 Bergen, Norway*
[5]*Lawrence Berkeley National Laboratory and University of California, Berkeley, California 94720, USA*
[6]*Ruhr Universität Bochum, Institut für Experimentalphysik 1, D-44780 Bochum, Germany*
[7]*University of British Columbia, Vancouver, British Columbia, Canada V6T 1Z1*
[8]*Brunel University, Uxbridge, Middlesex UB8 3PH, United Kingdom*
[9]*Budker Institute of Nuclear Physics, Novosibirsk 630090, Russia*
[10]*University of California at Irvine, Irvine, California 92697, USA*
[11]*University of California at Riverside, Riverside, California 92521, USA*
[12]*University of California at Santa Barbara, Santa Barbara, California 93106, USA*
[13]*University of California at Santa Cruz, Institute for Particle Physics, Santa Cruz, California 95064, USA*
[14]*California Institute of Technology, Pasadena, California 91125, USA*
[15]*University of Cincinnati, Cincinnati, Ohio 45221, USA*
[16]*University of Colorado, Boulder, Colorado 80309, USA*
[17]*Colorado State University, Fort Collins, Colorado 80523, USA*
[18]*Technische Universität Dortmund, Fakultät Physik, D-44221 Dortmund, Germany*
[19]*Technische Universität Dresden, Institut für Kern- und Teilchenphysik, D-01062 Dresden, Germany*
[20]*Laboratoire Leprince-Ringuet, Ecole Polytechnique, CNRS/IN2P3, F-91128 Palaiseau, France*
[21]*University of Edinburgh, Edinburgh EH9 3JZ, United Kingdom*
[22a]*INFN Sezione di Ferrara, I-44100 Ferrara, Italy*
[22b]*Dipartimento di Fisica, Università di Ferrara, I-44100 Ferrara, Italy*
[23]*INFN Laboratori Nazionali di Frascati, I-00044 Frascati, Italy*
[24a]*INFN Sezione di Genova, I-16146 Genova, Italy*
[24b]*Dipartimento di Fisica, Università di Genova, I-16146 Genova, Italy*
[25]*Indian Institute of Technology Guwahati, Guwahati, Assam, 781 039, India*
[26]*Harvard University, Cambridge, Massachusetts 02138, USA*
[27]*Harvey Mudd College, Claremont, California 91711, USA*
[28]*Universität Heidelberg, Physikalisches Institut, Philosophenweg 12, D-69120 Heidelberg, Germany*
[29]*Humboldt-Universität zu Berlin, Institut für Physik, Newtonstrasse 15, D-12489 Berlin, Germany*
[30]*Imperial College London, London, SW7 2AZ, United Kingdom*
[31]*University of Iowa, Iowa City, Iowa 52242, USA*
[32]*Iowa State University, Ames, Iowa 50011-3160, USA*
[33]*Johns Hopkins University, Baltimore, Maryland 21218, USA*
[34]*Laboratoire de l'Accélérateur Linéaire, IN2P3/CNRS et Université Paris-Sud 11, Centre Scientifique d'Orsay, B.P. 34, F-91898 Orsay Cedex, France*
[35]*Lawrence Livermore National Laboratory, Livermore, California 94550, USA*
[36]*University of Liverpool, Liverpool L69 7ZE, United Kingdom*
[37]*Queen Mary, University of London, London, E1 4NS, United Kingdom*
[38]*University of London, Royal Holloway and Bedford New College, Egham, Surrey TW20 0EX, United Kingdom*
[39]*University of Louisville, Louisville, Kentucky 40292, USA*
[40]*Johannes Gutenberg-Universität Mainz, Institut für Kernphysik, D-55099 Mainz, Germany*
[41]*University of Manchester, Manchester M13 9PL, United Kingdom*
[42]*University of Maryland, College Park, Maryland 20742, USA*
[43]*University of Massachusetts, Amherst, Massachusetts 01003, USA*
[44]*Massachusetts Institute of Technology, Laboratory for Nuclear Science, Cambridge, Massachusetts 02139, USA*
[45]*McGill University, Montréal, Québec, Canada H3A 2T8*
[46a]*INFN Sezione di Milano, I-20133 Milano, Italy*
[46b]*Dipartimento di Fisica, Università di Milano, I-20133 Milano, Italy*
[47]*University of Mississippi, University, Mississippi 38677, USA*
[48]*Université de Montréal, Physique des Particules, Montréal, Québec, Canada H3C 3J7*
[49a]*INFN Sezione di Napoli, I-80126 Napoli, Italy*
[49b]*Dipartimento di Scienze Fisiche, Università di Napoli Federico II, I-80126 Napoli, Italy*
[50]*NIKHEF, National Institute for Nuclear Physics and High Energy Physics, NL-1009 DB Amsterdam, Netherlands*

[51]*University of Notre Dame, Notre Dame, Indiana 46556, USA*
[52]*Ohio State University, Columbus, Ohio 43210, USA*
[53]*University of Oregon, Eugene, Oregon 97403, USA*
[54a]*INFN Sezione di Padova, I-35131 Padova, Italy*
[54b]*Dipartimento di Fisica, Università di Padova, I-35131 Padova, Italy*
[55]*Laboratoire de Physique Nucléaire et de Hautes Energies, IN2P3/CNRS, Université Pierre et Marie Curie-Paris6,*
Université Denis Diderot-Paris7, F-75252 Paris, France
[56a]*INFN Sezione di Perugia, I-06100 Perugia, Italy*
[56b]*Dipartimento di Fisica, Università di Perugia, I-06100 Perugia, Italy*
[57a]*INFN Sezione di Pisa, I-56127 Pisa, Italy*
[57b]*Dipartimento di Fisica, Università di Pisa, I-56127 Pisa, Italy*
[57c]*Scuola Normale Superiore di Pisa, I-56127 Pisa, Italy*
[58]*Princeton University, Princeton, New Jersey 08544, USA*
[59a]*INFN Sezione di Roma, I-00185 Roma, Italy*
[59b]*Dipartimento di Fisica, Università di Roma La Sapienza, I-00185 Roma, Italy*
[60]*Universität Rostock, D-18051 Rostock, Germany*
[61]*Rutherford Appleton Laboratory, Chilton, Didcot, Oxon, OX11 0QX, United Kingdom*
[62]*CEA, Irfu, SPP, Centre de Saclay, F-91191 Gif-sur-Yvette, France*
[63]*SLAC National Accelerator Laboratory, Stanford, California 94309 USA*
[64]*University of South Carolina, Columbia, South Carolina 29208, USA*
[65]*Southern Methodist University, Dallas, Texas 75275, USA*
[66]*Stanford University, Stanford, California 94305-4060, USA*
[67]*State University of New York, Albany, New York 12222, USA*
[68]*Tel Aviv University, School of Physics and Astronomy, Tel Aviv, 69978, Israel*
[69]*University of Tennessee, Knoxville, Tennessee 37996, USA*
[70]*University of Texas at Austin, Austin, Texas 78712, USA*
[71]*University of Texas at Dallas, Richardson, Texas 75083, USA*
[72a]*INFN Sezione di Torino, I-10125 Torino, Italy*
[72b]*Dipartimento di Fisica Sperimentale, Università di Torino, I-10125 Torino, Italy*
[73a]*INFN Sezione di Trieste, I-34127 Trieste, Italy*
[73b]*Dipartimento di Fisica, Università di Trieste, I-34127 Trieste, Italy*
[74]*IFIC, Universitat de Valencia-CSIC, E-46071 Valencia, Spain*
[75]*University of Victoria, Victoria, British Columbia, Canada V8W 3P6*
[76]*Department of Physics, University of Warwick, Coventry CV4 7AL, United Kingdom*
[77]*University of Wisconsin, Madison, Wisconsin 53706, USA*

In a sample of 471×10^6 $B\bar{B}$ events collected with the *BABAR* detector at the PEP-II e^+e^- collider we study the rare decays $B \to K^{(*)}\ell^+\ell^-$, where $\ell^+\ell^-$ is either e^+e^- or $\mu^+\mu^-$. We report results on partial branching fractions and isospin asymmetries in seven bins of dilepton mass-squared. We further present *CP* and lepton-flavor asymmetries for dilepton masses below and above the J/ψ resonance. We find no evidence for *CP* or lepton-flavor violation. The partial branching fractions and isospin asymmetries are consistent with the Standard Model predictions and with results from other experiments.

I. INTRODUCTION

The decays $B \to K^{(*)}\ell^+\ell^-$ arise from flavor-changing neutral-current processes that are forbidden at tree level in the Standard Model (SM). The lowest-order SM processes contributing to these decays are the photon penguin, the Z penguin and the W^+W^- box diagrams shown in Fig. 1. Their amplitudes are expressed in terms of hadronic form factors and perturbatively calculable effective Wilson coefficients, C_7^{eff}, C_9^{eff} and C_{10}^{eff}, which represent the electromagnetic penguin diagram, and the vector part and the axial-vector part of the linear combination of the Z penguin and W^+W^- box diagrams, respectively [1]. In next-to-next-to-leading order at a renormalization scale $\mu = 4.8$ GeV, the effective Wilson coefficients are $C_7^{\mathrm{eff}} = -0.304$, $C_9^{\mathrm{eff}} = 4.211$, and $C_{10}^{\mathrm{eff}} = -4.103$ [2].

Non-SM physics may add new penguin and box diagrams, which can contribute at the same order as the SM

---

*Now at the University of Tabuk, Tabuk 71491, Saudi Arabia.
†Also with Università di Perugia, Dipartimento di Fisica, Perugia, Italy.
‡Now at the University of Huddersfield, Huddersfield HD1 3DH, United Kingdom.
§Now at University of South Alabama, Mobile, AL 36688, USA.
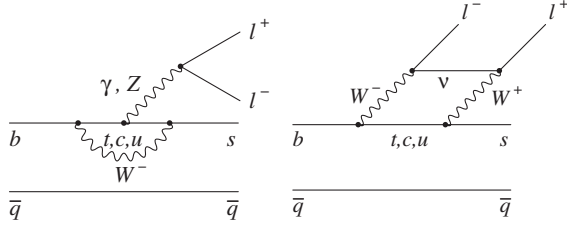‖Also with Università di Sassari, Sassari, Italy.

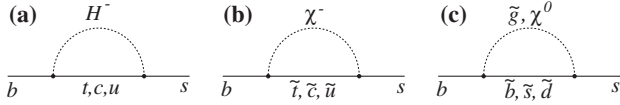FIG. 1.   Lowest-order Feynman diagrams for $b \rightarrow s\ell^+\ell^-$.

FIG. 2.   Examples of new physics loop contributions to $b \rightarrow s\ell^+\ell^-$: (a) charged Higgs ($H^-$); (b) squark ($\tilde{t}, \tilde{c}, \tilde{u}$) and chargino ($\chi^-$); (c) squark ($\tilde{b}, \tilde{s}, \tilde{d}$) and gluino ($\tilde{g}$) or neutralino ($\chi^0$).

diagrams [3–5]. Examples of new physics loop processes are depicted in Fig. 2. These contributions might modify the Wilson coefficients from their SM expectations [5–7]. In addition, new contributions from scalar, pseudoscalar, and tensor currents may arise that can modify, in particular, the lepton-flavor ratios [8,9].

II. OBSERVABLES

We report herein results on exclusive partial branching fractions and isospin asymmetries in six bins of $s \equiv m_{\ell\ell}^2$, defined in Table I. We further present results in the s bin $s_0 = 1.0$–6.0 GeV$^2/c^4$ chosen for calculations inspired by soft-collinear effective theory [10]. In addition, we report on direct CP asymmetries and the ratio of rates to dimuon and dielectron final states in the low s and high s regions separated by the J/ψ resonance. We remove regions of the long-distance contributions around the J/ψ and $\psi(2S)$ resonances. New *BABAR* results on angular observables using the same data set and similar event selection will be reported shortly.

The $B \rightarrow K\ell^+\ell^-$ and $B \rightarrow K^*\ell^+\ell^-$ total branching fractions are predicted to be $(0.35 \pm 0.12) \times 10^{-6}$ and $(1.19 \pm 0.39) \times 10^{-6}$ (for $s > 0.1$ GeV$^2/c^4$), respectively [5]. The $\sim 30\%$ uncertainties are due to a lack of knowledge about the form factors that model the hadronic effects in the $B \rightarrow K$ and $B \rightarrow K^*$ transitions. Thus, measurements of decay rates to exclusive final states are less suited to searches for new physics than rate asymmetries, where many theory uncertainties cancel.

For charged B decays and neutral B decays flavor-tagged through $K^* \rightarrow K^+\pi^-$ [11], the direct CP asymmetry is defined as

$$\mathcal{A}_{CP}^{K^{(*)}} \equiv \frac{\mathcal{B}(\bar{B} \rightarrow \bar{K}^{(*)}\ell^+\ell^-) - \mathcal{B}(B \rightarrow K^{(*)}\ell^+\ell^-)}{\mathcal{B}(\bar{B} \rightarrow \bar{K}^{(*)}\ell^+\ell^-) + \mathcal{B}(B \rightarrow K^{(*)}\ell^+\ell^-)} \quad (1)$$

and is expected to be $\mathcal{O}(10^{-3})$ in the SM. However $\mathcal{A}_{CP}^{K^{(*)}}$ may receive a significant enhancement from new physics contributions at the electroweak scale [12].

TABLE I.   The definition of seven s bins used in the analysis. Here m_B and $m_{K^{(*)}}$ are the invariant masses of B and $K^{(*)}$, respectively. The low s region is given by $0.10 < s < 8.12$ GeV$^2/c^4$, while the high s region is given by $s > 10.11$ GeV$^2/c^4$.

	s bin	s min (GeV$^2/c^4$)	s max (GeV$^2/c^4$)
Low	s_1	0.10	2.00
	s_2	2.00	4.30
	s_3	4.30	8.12
High	s_4	10.11	12.89
	s_5	14.21	16.00
	s_6	16.00	$(m_B - m_{K^{(*)}})^2$
	s_0	1.00	6.00

For $s > 0.1$ GeV$^2/c^4$, the ratio of rates to dimuon and dielectron final states is defined as

$$\mathcal{R}_{K^{(*)}} \equiv \frac{\mathcal{B}(B \rightarrow K^{(*)}\mu^+\mu^-)}{\mathcal{B}(B \rightarrow K^{(*)}e^+e^-)}. \quad (2)$$

In the SM, $\mathcal{R}_{K^{(*)}}$ is expected to be unity to within a few percent [13] for dilepton invariant masses above the dimuon kinematic threshold. In two-Higgs-doublet models, including supersymmetry, these ratios are sensitive to the presence of a neutral Higgs boson. When the ratio of neutral Higgs field vacuum expectation values $\tan\beta$ is large, $\mathcal{R}_{K^{(*)}}$ might be increased by up to 10% [9].

The CP-averaged isospin asymmetry is defined as

$$\mathcal{A}_I^{K^{(*)}} \equiv \frac{\mathcal{B}(B^0 \rightarrow K^{(*)0}\ell^+\ell^-) - r_\tau \mathcal{B}(B^+ \rightarrow K^{(*)+}\ell^+\ell^-)}{\mathcal{B}(B^0 \rightarrow K^{(*)0}\ell^+\ell^-) + r_\tau \mathcal{B}(B^+ \rightarrow K^{(*)+}\ell^+\ell^-)}, \quad (3)$$

where $r_\tau \equiv \tau_{B^0}/\tau_{B^+} = 1/(1.071 \pm 0.009)$ is the ratio of B^0 and B^+ lifetimes [14]. $\mathcal{A}_I^{K^*}$ has a SM expectation of $+6\%$ to $+13\%$ as $s \rightarrow 0$ [4]. This is consistent with the measured asymmetry $3 \pm 3\%$ in $B \rightarrow K^*\gamma$ [15]. A calculation of the predicted K^{*+} and K^{*0} rates integrated over the low s region yields $\mathcal{A}_I^{K^*} = -0.005 \pm 0.020$ [16,17]. In the high s region, we may expect contributions from charmonium states as an additional source of isospin asymmetry. However the measured asymmetries in the $J/\psi K^{(*)}$ and $\psi(2S)K^{(*)}$ modes are all below 5% [14].

III. *BABAR* EXPERIMENT AND DATA SAMPLE

We use a data sample of 471×10^6 $B\bar{B}$ pairs collected at the $\Upsilon(4S)$ resonance with the *BABAR* detector [18] at the PEP-II asymmetric-energy e^+e^- collider at the SLAC National Accelerator Laboratory. Charged particle tracking is provided by a five-layer silicon vertex tracker and a 40-layer drift chamber in a 1.5 T solenoidal magnetic field. We identify electrons with a CsI(Tl) electromagnetic calorimeter, and muons using an instrumented magnetic flux return. Electron and muon candidates are required to have

momenta $p > 0.3$ GeV/c in the laboratory frame. We combine up to three photons with electrons when they are consistent with bremsstrahlung, and do not use electrons that are associated with photon conversions to low-mass e^+e^- pairs. We identify charged kaons using a detector of internally reflected Cherenkov light, as well as dE/dx information from the drift chamber. Charged tracks other than identified e, μ and K candidates are treated as pions. Neutral $K_S^0 \to \pi^+\pi^-$ candidates are required to have an invariant mass consistent with the nominal K^0 mass, and a flight distance from the e^+e^- interaction point that is more than 3 times its uncertainty.

IV. EVENT SELECTION

We reconstruct $B \to K^{(*)}\ell^+\ell^-$ signal events in the following eight final states:
(i) $B^0 \to K_S^0\mu^+\mu^-$,
  $B^+ \to K^+\mu^+\mu^-$,
  $B^0 \to K_S^0e^+e^-$,
  $B^+ \to K^+e^+e^-$,
  $B^+ \to K^{*+}(\to K_S^0\pi^+)\mu^+\mu^-$,
  $B^0 \to K^{*0}(\to K^+\pi^-)\mu^+\mu^-$,
  $B^+ \to K^{*+}(\to K_S^0\pi^+)e^+e^-$,
  $B^0 \to K^{*0}(\to K^+\pi^-)e^+e^-$.

We reconstruct K_S^0 candidates in the $\pi^+\pi^-$ final state. We also study the $K^{(*)}h^\pm\mu^\mp$ final states, where h is a charged track with no particle identification requirement applied, to characterize backgrounds from hadrons misidentified as muons. We use a $K^*e^\pm\mu^\mp$ sample to model the combinatorial background from two random leptons. In each mode, we utilize the kinematic variables $m_{\rm ES} = \sqrt{E_{\rm CM}^2/4 - p_B^{*2}}$ and $\Delta E = E_B^* - E_{\rm CM}/2$, where p_B^* and E_B^* are the B momentum and energy in the $\Upsilon(4S)$ center-of-mass (CM) frame, and $E_{\rm CM}$ is the total CM energy.

For masses $m_{\rm ES} > 5.2$ GeV/c^2 we perform one-dimensional fits of the $m_{\rm ES}$ distribution for $K\ell^+\ell^-$ modes. For $K^*\ell^+\ell^-$ modes, we include in addition the $K\pi$ mass region $0.72 < m_{K\pi} < 1.10$ GeV/c^2 in the fit. We use the sideband $5.20 < m_{\rm ES} < 5.27$ GeV/c^2 to characterize combinatorial background shapes and normalizations. For both the e^+e^- and $\mu^+\mu^-$ modes, we veto the $J/\psi (2.85 < m_{\ell\ell} < 3.18$ GeV/c^2) and $\psi(2S) \times (3.59 < m_{\ell\ell} < 3.77$ GeV/c^2) mass regions. The vetoed events provide high-statistics control samples that we use to validate the fit methodology.

The main backgrounds arise from random combinations of leptons from semileptonic B and D decays. These combinatorial backgrounds from either $B\bar{B}$ events (referred to as "$B\bar{B}$ backgrounds") or continuum $q\bar{q}$ events ($e^+e^- \to q\bar{q}$, $q = u, d, s, c$, referred to as "$q\bar{q}$ backgrounds") are suppressed using bagged decision trees (BDTs) [19]. We train eight separate BDTs as follows:

(i) suppression of $B\bar{B}$ backgrounds for e^+e^- modes in the low s region;
(ii) suppression of $B\bar{B}$ backgrounds for e^+e^- modes in the high s region;
(iii) suppression of $B\bar{B}$ backgrounds for $\mu^+\mu^-$ modes in the low s region;
(iv) suppression of $B\bar{B}$ backgrounds for $\mu^+\mu^-$ modes in the high s region;
(v) suppression of $q\bar{q}$ backgrounds for e^+e^- modes in the low s region;
(vi) suppression of $q\bar{q}$ backgrounds for e^+e^- modes in the high s region;
(vii) suppression of $q\bar{q}$ backgrounds for $\mu^+\mu^-$ modes in the low s region;
(viii) suppression of $q\bar{q}$ backgrounds for $\mu^+\mu^-$ modes in the high s region.

The BDT input parameters include the following observables:
(i) ΔE of the B candidate;
(ii) the ratio of Fox-Wolfram moments R_2 [20] and the ratio of the second-to-zeroth angular moments of the energy flow L_2/L_0 [21], both event shape parameters calculated using charged and neutral particles in the CM frame;
(iii) the mass and ΔE of the other B meson in the event (referred to as the "rest of the event") computed in the laboratory frame by summing the momenta and energies of all charged particles and photons that are not used to reconstruct the signal candidate;
(iv) the magnitude of the total transverse momentum of the event in the laboratory frame;
(v) the probabilities that the B candidate and the dilepton candidate, respectively, originate from a single point in space;
(vi) the cosine values of four angles: the angle between the B candidate momentum and the beam axis, the angle between the event thrust axis and the beam axis, the angle between the thrust axis of the rest of the event and the beam axis, and the angle between the event thrust axis and the thrust axis of the rest of the event, all defined in the CM frame.

Figure 3 shows the output distributions of the BDTs for Monte Carlo (MC) simulated signal and combinatorial background for the e^+e^- sample below the J/ψ resonance. The distributions are histograms normalized to unit area. The selections on BDT outputs are further optimized to maximize the statistical significance of the signal events, as shown later.

Another source of background arises from $B \to D(\to K^{(*)}\pi)\pi$ decays if both pions are misidentified as leptons. Determined from data control samples with high purity [18], the misidentification rates for muons and electrons are $\sim 3\%$ and $\lesssim 0.1\%$ per candidate, respectively. Thus, this background is only significant for $\mu^+\mu^-$
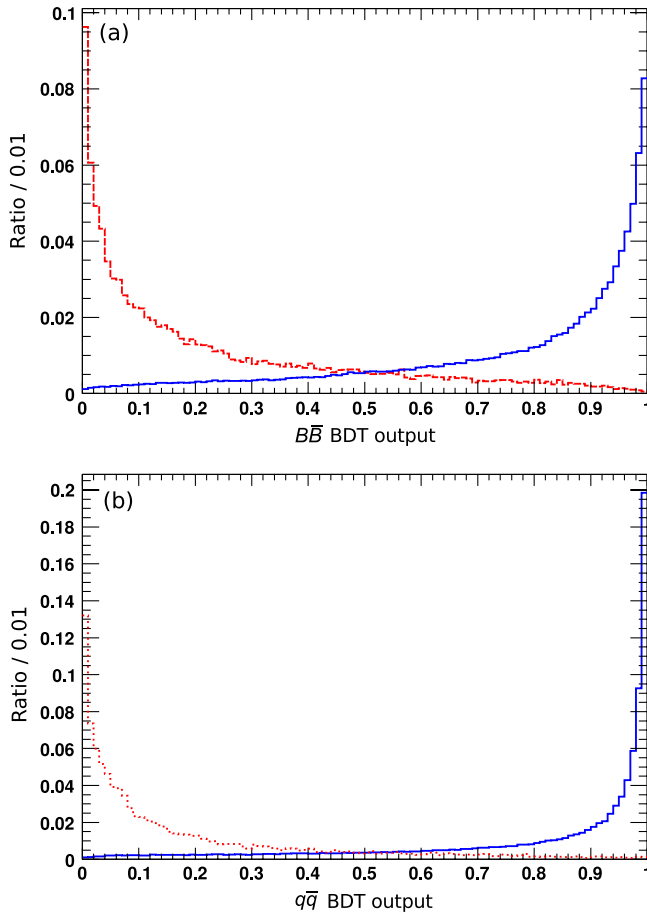
FIG. 3 (color online). The (a) $B\bar{B}$ and (b) $q\bar{q}$ e^+e^- BDT outputs for simulated events in the low s region. Shown are the distributions for $B\bar{B}$ background (red dashed line), $q\bar{q}$ background (red dotted line), and signal (blue solid line) event samples, normalized to unit area.

final states. We veto these events by requiring the invariant mass of the $K^{(*)}\pi$ system to be outside the range 1.84–1.90 GeV/c^2 after assigning the pion mass hypothesis to the muon candidates. Any remaining residual backgrounds from this type of contribution are parameterized using control samples obtained from data.

After applying all selection criteria about 85% of signal events contain more than one B candidate. These candidates differ typically in one charged or neutral hadron. The average number of candidates per signal event is about six. To choose the best candidate, we define the ratio

$$\lambda \equiv \frac{\mathcal{P}^{B\bar{B}}_{\text{sig}} + \mathcal{P}^{q\bar{q}}_{\text{sig}}}{\mathcal{P}^{B\bar{B}}_{\text{sig}} + \mathcal{P}^{q\bar{q}}_{\text{sig}} + \mathcal{P}^{B\bar{B}}_{\text{bkg}} + \mathcal{P}^{q\bar{q}}_{\text{bkg}}}, \qquad (4)$$

where $\mathcal{P}_{\text{sig}}$ and $\mathcal{P}_{\text{bkg}}$ are probabilities calculated from the corresponding $B\bar{B}$ and $q\bar{q}$ BDT output distributions for signal and background, respectively. We select the candidate with the largest λ as the best candidate. The probability for a correctly reconstructed signal event to be

selected as the best candidate is mode-dependent and varies between about 80% and 95% for s bins below the J/ψ mass, while for s bins above the $\psi(2S)$ mass it varies between about 60% and 90%.

V. SELECTION OPTIMIZATION

To optimize the ΔE selection, we simultaneously vary the upper and lower bounds of the ΔE interval to find the values that maximize the ratio $S/\sqrt{S+B}$ in the signal region ($m_{\text{ES}} > 5.27$ GeV/c^2, and for K^* modes in addition $0.78 < m_{K\pi} < 0.97$ GeV/c^2), where S and B are the expected numbers [14] of signal and combinatorial background events, respectively. We perform separate optimizations for dilepton masses below and above the J/ψ mass. For some modes, the optimization tends to select very narrow intervals, which leads to small signal efficiency. To prevent this, we require the magnitudes of the ΔE upper and lower bounds to be 0.04 GeV or larger. (Note that the lower bound is always negative and the upper bound always positive.)

We also optimize the lower bounds on the BDT $B\bar{B}$ and $q\bar{q}$ intervals (the upper bounds on these intervals are always 1.0). We perform fits to extract signal yields using the fit model described in Sec. VI. For each mode, the lower bound on the BDT interval is optimized by maximizing the expected signal significance defined as the fitted signal yield divided by its associated uncertainty. We determine these from 500 pseudoexperiments using branching fraction averages [14]. The optimized BDT lower bounds are listed in Tables II and III for $K\ell^+\ell^-$ and $K^*\ell^+\ell^-$, respectively. Figure 4 shows the expected experimental significance in the $B\bar{B}$ BDT versus the $q\bar{q}$ BDT plane for $B^0 \to K^+\pi^-\mu^+\mu^-$ in bin s_2. The signal selection efficiency and the cross-feed fraction (defined in Sec. VI) in each mode and s bin after the final event selection are also listed in Tables II and III. The selection efficiencies determined in simulations vary from $11.4 \pm 0.2\%$ for $K_S^0\pi^+e^+e^-$ in s_6 to $33.3 \pm 0.3\%$ for $K^+\mu^+\mu^-$ in s_5, where the uncertainties are statistical.

VI. FIT METHODOLOGY

We perform one-dimensional fits in m_{ES} for $K\ell^+\ell^-$ modes and two-dimensional fits in m_{ES} and $m_{K\pi}$ for $K^*\ell^+\ell^-$ modes to extract the signal yields. The probability density function (PDF) for signal m_{ES} is parametrized by a Gaussian function with mean and width fixed to values obtained from fits to the vetoed J/ψ events in the data control samples. For $m_{K\pi}$, the PDF is a relativistic Breit-Wigner line shape [22]. True signal events are those where all generator-level final-state daughter particles are correctly reconstructed and are selected to form a B candidate.

For the combinatorial background, the m_{ES} PDF is modeled with a kinematic threshold function whose shape is a free parameter in the fits [23], while the $m_{K\pi}$ PDF shape is

TABLE II.   Optimized lower bounds on the BDT intervals, signal reconstruction efficiency, and cross-feed fraction, by $K\ell^+\ell^-$ mode and s bin. The uncertainties are statistical only.

Mode	s bin	$B\bar{B}$ BDT	$q\bar{q}$ BDT	Efficiency [%]	Cross-feed fraction [%]
$B^0 \rightarrow K_S^0 \mu^+ \mu^-$	s_1	0.20	0.80	19.9 ± 0.2	8.9 ± 0.3
	s_2	0.70	0.85	22.2 ± 0.2	8.6 ± 0.2
	s_3	0.20	0.85	25.2 ± 0.1	8.9 ± 0.2
	s_4	0.70	0.70	24.3 ± 0.2	9.4 ± 0.2
	s_5	0.70	0.80	22.2 ± 0.2	12.0 ± 0.5
	s_6	0.75	0.80	16.6 ± 0.1	21.7 ± 0.7
	s_0	0.50	0.85	22.7 ± 0.1	8.8 ± 0.1
$B^+ \rightarrow K^+ \mu^+ \mu^-$	s_1	0.30	0.85	21.3 ± 0.2	0.3 ± 0.0
	s_2	0.15	0.85	27.0 ± 0.2	0.3 ± 0.0
	s_3	0.15	0.85	30.9 ± 0.1	0.3 ± 0.0
	s_4	0.80	0.85	31.0 ± 0.2	0.4 ± 0.0
	s_5	0.65	0.85	33.3 ± 0.3	2.1 ± 0.1
	s_6	0.05	0.85	30.5 ± 0.2	10.4 ± 0.2
	s_0	0.05	0.85	13.6 ± 0.1	0.3 ± 0.0
$B^0 \rightarrow K_S^0 e^+ e^-$	s_1	0.25	0.80	22.1 ± 0.2	8.3 ± 0.3
	s_2	0.25	0.80	25.2 ± 0.2	9.4 ± 0.3
	s_3	0.65	0.80	24.3 ± 0.1	9.4 ± 0.2
	s_4	0.50	0.85	24.1 ± 0.2	10.9 ± 0.4
	s_5	0.05	0.65	23.0 ± 0.2	18.5 ± 0.9
	s_6	0.25	0.70	16.5 ± 0.1	35.0 ± 1.1
	s_0	0.85	0.85	21.3 ± 0.1	9.2 ± 0.2
$B^+ \rightarrow K^+ e^+ e^-$	s_1	0.35	0.85	22.8 ± 0.2	0.4 ± 0.1
	s_2	0.10	0.85	28.8 ± 0.2	0.4 ± 0.0
	s_3	0.10	0.85	30.8 ± 0.1	0.5 ± 0.0
	s_4	0.30	0.80	32.7 ± 0.2	1.1 ± 0.1
	s_5	0.25	0.80	31.7 ± 0.3	4.3 ± 0.2
	s_6	0.50	0.85	25.1 ± 0.2	12.0 ± 0.3
	s_0	0.40	0.85	29.6 ± 0.1	0.5 ± 0.0

characterized with the $K^* e^\pm \mu^\mp$ sample mentioned in Sec. IV. We parameterize the combinatorial $m_{K\pi}$ distributions with nonparametric Gaussian kernel density estimator shapes [24] (referred to as the "KEYS PDFs") drawn from the $K^* e^\pm \mu^\mp$ sample in the full m_{ES} fit region. Since the correlation between $m_{K\pi}$ and ΔE is weak, we accept all $K^* e^\pm \mu^\mp$ events within $|\Delta E| < 0.3$ GeV, rather than imposing a stringent ΔE selection, in order to enhance sample sizes.

Signal cross feed consists of misreconstructed signal events, in which typically a low-momentum $\pi^\pm$ or π^0 is swapped, added, or removed in the B candidate reconstruction. We distinguish among different categories of cross feed: "self-cross-feed" is when a particle is swapped within one mode, "feed-across" is when a particle is swapped between two signal modes with the same final-state multiplicity, and "feed-up (-down)" is when a particle is added (removed) from a lower (higher) multiplicity $b \rightarrow s\ell^+\ell^-$ mode. We use both exclusive and inclusive $b \rightarrow s\ell^+\ell^-$ MC samples to evaluate the contributions of the different categories. The cross-feed m_{ES} distribution is typically broadened compared to correctly reconstructed signal decays. We combine the cross-feed contributions

from all sources into a single fit component that is modeled as a sum of weighted histograms with a single overall normalization, which is allowed to scale as a fixed fraction of the observed correctly reconstructed signal yield. This fixed fraction is presented as the "cross-feed fraction" in Tables II and III. The modeling of cross-feed contributions is validated using fits to the vetoed $J/\psi K^{(*)}$ and $\psi(2S)K^{(*)}$ events, in which the cross-feed contributions are relatively large compared to all other backgrounds.

Exclusive B hadronic decays may be misreconstructed as $B \rightarrow K^{(*)}\ell^+\ell^-$, since hadrons can be misidentified as muons. Following a procedure similar to that described in Ref. [25], we determine this background by selecting a sample of $K^{(*)}\mu^\pm h^\mp$ events, in which the muon is identified as a muon and the hadron is inconsistent with an electron. Requiring identified kaons and pions, we select subsamples of $K^{(*)}\pi^+\pi^-$, $K^{(*)}K^+\pi^-$, $K^{(*)}\pi^+K^-$, and $K^{(*)}K^+K^-$. We obtain weights from data control samples where a charged particle's species can be identified with high precision and accuracy without using particle identification information. The weights are then applied to this data set to characterize the contribution expected in our fits

TABLE III. Optimized lower bounds on the BDT intervals, signal reconstruction efficiency, and cross-feed fraction, by $K^* \ell^+ \ell^-$ mode and s bin. The uncertainties are statistical only.

Mode	s bin	$B\bar{B}$ BDT	$q\bar{q}$ BDT	Efficiency [%]	Cross-feed fraction [%]
$B^+ \to K_S^0 \pi^+ \mu^+ \mu^-$	s_1	0.55	0.85	13.6 ± 0.1	14.0 ± 0.5
	s_2	0.80	0.85	14.6 ± 0.2	19.2 ± 0.7
	s_3	0.85	0.80	14.9 ± 0.1	20.7 ± 0.5
	s_4	0.85	0.85	14.7 ± 0.1	28.0 ± 0.7
	s_5	0.15	0.85	16.4 ± 0.2	59.3 ± 1.3
	s_6	0.10	0.85	14.3 ± 0.1	110.8 ± 1.9
	s_0	0.80	0.85	14.5 ± 0.1	18.9 ± 0.5
$B^0 \to K^+ \pi^- \mu^+ \mu^-$	s_1	0.80	0.85	16.2 ± 0.1	4.9 ± 0.2
	s_2	0.80	0.85	19.6 ± 0.2	7.8 ± 0.3
	s_3	0.75	0.85	21.3 ± 0.1	10.1 ± 0.2
	s_4	0.85	0.85	20.9 ± 0.1	13.8 ± 0.3
	s_5	0.75	0.85	22.8 ± 0.2	31.7 ± 0.6
	s_6	0.80	0.80	19.5 ± 0.2	61.0 ± 0.9
	s_0	0.60	0.85	20.4 ± 0.1	8.9 ± 0.2
$B^+ \to K_S^0 \pi^+ e^+ e^-$	s_1	0.45	0.70	16.6 ± 0.2	17.8 ± 0.6
	s_2	0.85	0.85	13.7 ± 0.2	20.7 ± 0.8
	s_3	0.55	0.85	16.0 ± 0.1	27.5 ± 0.7
	s_4	0.40	0.85	15.4 ± 0.1	41.6 ± 0.9
	s_5	0.80	0.45	13.1 ± 0.2	68.6 ± 1.8
	s_6	0.60	0.85	11.4 ± 0.2	133.4 ± 2.9
	s_0	0.70	0.85	16.0 ± 0.1	23.1 ± 0.5
$B^0 \to K^+ \pi^- e^+ e^-$	s_1	0.80	0.85	16.5 ± 0.2	6.8 ± 0.2
	s_2	0.85	0.85	18.6 ± 0.2	10.9 ± 0.3
	s_3	0.80	0.80	18.5 ± 0.1	11.2 ± 0.3
	s_4	0.55	0.65	21.9 ± 0.2	25.6 ± 0.4
	s_5	0.75	0.80	19.0 ± 0.2	50.4 ± 0.9
	s_6	0.05	0.80	15.1 ± 0.2	110.9 ± 1.8
	s_0	0.80	0.85	19.7 ± 0.1	10.8 ± 0.2

due to misidentified muon candidates. We characterize the misidentification backgrounds using the KEYS PDFs, with normalizations obtained by construction directly from the weighted data.

Some charmonium events may escape the charmonium vetoes and appear in our fit region. Typically, this occurs when electrons radiate a photon or a muon candidate is a misidentified hadron and the missing energy is accounted for by a low-energy $\pi^\pm$ or π^0. The largest background contributions from this source are expected in the $K^* \mu^+ \mu^-$ and $K^* e^+ e^-$ channels. We model this background using the charmonium MC samples and determine the leakage into s bins on either side of the J/ψ and $\psi(2S)$ resonances. We see a notable charmonium contribution (about five events) for $B^0 \to K^+ \pi^- \mu^+ \mu^-$ in bin s_3. This leakage is typically caused by a swap between the μ^+ and π^+ in a single $B \to J/\psi(\to \mu^+ \mu^-) K \pi^+$ candidate, where both the μ^+ and π^+ are misidentified.

Hadronic peaking background from $B \to K^* \pi^0$ and $B \to K^* \eta$ in which the π^0 or η decays via Dalitz pairs shows a small peaking component in m_{ES} in bin s_1. Because of the requirement $s > 0.1$ GeV$^2/c^4$, contributions of γ

conversions from $B \to K^* \gamma$ events beyond the photon pole region are found to be negligible.

Fit model for rate asymmetries

Using the PDFs described above, we perform simultaneous fits across different $K^{(*)} \ell^+ \ell^-$ modes. Since efficiency-corrected signal yields are shared across various decay modes, we can extract rate asymmetries directly from the fits. The fitted signal yields in B^+ modes are corrected by the lifetime ratio τ_{B^0}/τ_{B^+}. We also correct the signal yields for $\mathcal{B}(K^* \to K\pi)$ in K^* modes and $\mathcal{B}(K_S^0 \to \pi^+ \pi^-)$ in the modes with a K_S^0. In the fits for $\mathcal{A}_{CP}$, we share the efficiency-corrected signal yield N_B as a floating variable for B $q\bar{b}$, $q = u, d$ events across different flavor-tagging $K^{(*)} \ell^+ \ell^-$ modes by assuming lepton-flavor and isospin symmetries. The efficiency-corrected signal yield $N_{\bar{B}}$ for $\bar{B}(\bar{q}b)$ events is then defined by $N_{\bar{B}} = N_B \cdot (1 + \mathcal{A}_{CP})/(1 - \mathcal{A}_{CP})$ and is also shared across corresponding modes. For the lepton-flavor ratios $\mathcal{R}_{K^{(*)}}$, we share the efficiency-corrected signal yield N_{ee} as a floating variable for the two $B \to K e^+ e^-$ or
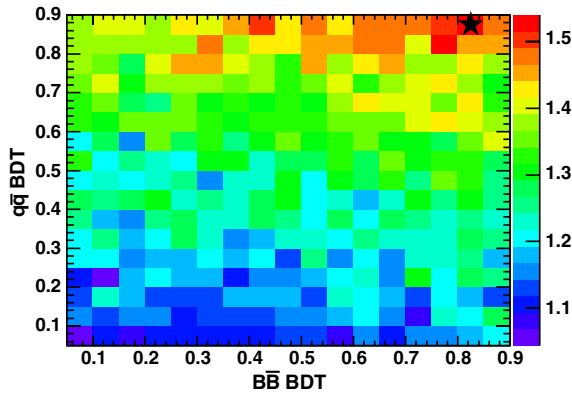
FIG. 4 (color online). Expected statistical significance of the number of fitted signal events as a function of BDT interval lower bounds for $B^0 \to K^+ \pi^- \mu^+ \mu^-$ in bin s_2. The star marks the optimized pair of lower bounds.

$B \to K^* e^+ e^-$ modes by assuming isospin symmetry. The efficiency-corrected signal yield $N_{\mu\mu}$ shared across the corresponding $B \to K^{(*)} \mu^+ \mu^-$ modes is then defined by $N_{\mu\mu} = N_{ee} \cdot R_{K^{(*)}}$. For the isospin asymmetry $\mathcal{A}_I^{K^{(*)}}$, we share the efficiency-corrected signal yield N_{B^+} as a floating variable for the two $B^+ \to K^+ \ell^+ \ell^-$ or $B^+ \to K^{*+} \ell^+ \ell^-$ modes by assuming lepton-flavor symmetry. The efficiency-corrected signal yield N_{B^0} shared across the corresponding $B^0 \to K^{*0} \ell^+ \ell^-$ modes is then defined by $N_{B^0} = N_{B^+} \cdot (1 + \mathcal{A}_I^{K^{(*)}}) / (1 - \mathcal{A}_I^{K^{(*)}})$.

VII. FIT VALIDATION

We validate the fit methodology with charmonium control samples obtained from the dilepton mass regions around the J/ψ and $\psi(2S)$ resonances that are vetoed in the $B \to K^{(*)} \ell^+ \ell^-$ analysis. We measure the $J/\psi K^{(*)}$ and $\psi(2S)K^{(*)}$ branching fractions in each final state with the optimized BDT selections in bins s_3 and s_4, respectively. Our measurements agree well with the world averages [14] for all final states. Typical deviations, based on statistical uncertainties only, are less than 1 standard deviation (σ). The largest deviation, in the $K^+ \pi^- \mu^+ \mu^-$ mode, is 1.7σ. For $J/\psi K^{(*)}$ modes, the statistical uncertainties are considerably smaller than those of the world averages. We float the Gaussian means and widths of the signal PDFs in the fits for the $J/\psi K^{(*)}$ modes. The associated uncertainties obtained from the fits are then used as a source of systematic variation for the signal PDFs. The typical signal width in $m_{\rm ES}$ is 2.5 MeV/c^2.

We further validate our fitting procedure by applying it to charmonium events to extract the rate asymmetries. The measured CP asymmetries $\mathcal{A}_{CP}$, lepton-flavor ratios $\mathcal{R}_{K^{(*)}}$ and isospin asymmetries $\mathcal{A}_I$ are in good agreement with Standard Model expectations or world averages for $\mathcal{A}_I$.

We also test the methodology with fits to ensembles of data sets where signal and background events are generated

from appropriately normalized PDFs ("pure pseudoexperiments"). We perform fits to these pseudoexperiments in each mode and s bin using the full fit model described previously. For ensembles of 1000 pure pseudoexperiments, the pull distributions for the signal yields show negligible biases. We further fit ensembles of pseudoexperiments in which the signal events are drawn from properly normalized exclusive MC samples ("embedded pseudoexperiments"). The pull distributions also show the expected performance.

We perform fits to ensembles of pure pseudoexperiments in order to estimate the statistical sensitivity of, and biases related to, the various rate asymmetry measurements. The pull distributions for $\mathcal{A}_{CP}$ and $\mathcal{R}_{K^{(*)}}$ for the low and high s regions show minimal biases. For $\mathcal{A}_I$, we test a series of $\mathcal{A}_I$ input values ($-0.6, -0.3, 0.0, 0.3, 0.6$) in each s bin using pure pseudoexperiments to ensure we obtain unbiased fits under different assumptions of isospin asymmetry. The $\mathcal{A}_I^K$ pulls are generally well-behaved. In the worst case, the test fits for $\mathcal{A}_I^K$ are slightly biased due to very low signal yield expectations in the $K_S^0 \ell^+ \ell^-$ final states.

VIII. SYSTEMATIC UNCERTAINTIES

Since some systematic uncertainties largely cancel in ratios, it is useful to separate the discussion of systematic uncertainties on partial branching fractions from that on rate asymmetries.

A. Branching Fraction Uncertainties

Systematic uncertainties for branching fractions arise from multiplicative systematic uncertainties involving the determination of the signal efficiency, and from additive systematic uncertainties arising from the extraction of signal yields in the data fits. The multiplicative systematic errors include contributions from the

(i)   Number of $B\bar{B}$ pairs: This uncertainty is 0.6%.
(ii) Tracking efficiency for charged particles: We assign a correlated uncertainty of 0.3% for each lepton, and 0.4% for each charged hadron including daughter pions from K_S^0 decay [26].
(iii) Charged particle identification (PID) efficiencies: We employ a data-driven method to correct PID efficiencies in simulated events. We estimate the systematic uncertainties from the change in signal efficiency for simulated $J/\psi K^{(*)}$ events after turning off the PID corrections. The systematic uncertainties are mode-dependent and vary between 0.3% and 1.6%.
(iv) K_S^0 identification efficiency: This is determined as a function of flight distance after applying K_S^0 efficiency corrections. An uncertainty of 0.9% is obtained by varying the K_S^0 selection algorithm.
(v)   Event selection efficiency: We measure the efficiency of the BDT selection in charmonium data

TABLE IV.   Individual systematic uncertainties [%] for measurements of the total branching fractions in $K^{(*)}\ell^+\ell^-$ decays.

Mode	$K_S^0\mu^+\mu^-$	$K^+\mu^+\mu^-$	$K_S^0 e^+e^-$	$K^+ e^+e^-$	$K_S^0\pi^+\mu^+\mu^-$	$K^+\pi^-\mu^+\mu^-$	$K_S^0\pi^+ e^+e^-$	$K^+\pi^- e^+e^-$
$B\bar{B}$ counting	±0.6	±0.6	±0.6	±0.6	±0.6	±0.6	±0.6	±0.6
Tracking	±1.4	±1.0	±1.4	±1.0	±1.8	±1.4	±1.8	±1.4
PID	±1.6	±0.3	±0.7	±0.4	±1.5	±0.3	±0.5	±1.2
K_s^0 ID	±0.9	⋯	±0.9	⋯	±0.9	⋯	±0.9	⋯
BDT selections	±2.2	±1.7	±4.7	±1.5	±8.3	±2.5	±9.1	±2.7
MC sample size	±0.3	±0.3	±0.3	±0.3	±0.4	±0.3	±0.4	±0.4
Sig. shape	±0.5	±0.4	±1.5	±0.4	±1.5	±0.7	±1.5	±0.7
Hadronic	±3.3	±5.8	⋯	⋯	±2.3	±1.6	⋯	⋯
Peaking	±0.3	±0.8	±1.2	±0.8	±0.7	±1.7	±0.8	±1.2
Comb. $m_{K\pi}$ shape	⋯	⋯	⋯	⋯	±1.2	±0.6	±0.6	±1.6
Total	±4.7	±6.3	±5.4	±2.2	±9.3	±3.9	±9.5	±4.0

control samples and compare with results obtained for exclusive charmonium samples from simulation. We take the magnitude of the deviation for any particular final state and s bin as the uncertainty associated with the BDT lower bounds. If the data and simulation are consistent within the uncertainty, we then take the uncertainty as the systematic uncertainty. The systematic uncertainty is found to vary between 0.3% and 9.1% depending on both the mode and the s bin. Because of a strong correlation between the ΔE and BDT outputs, uncertainties due to ΔE are fully accounted for by this procedure.

(vi) Monte Carlo sample size: We find the uncertainty related to the finite size of the MC sample to be of the order of 1% or less for all modes.

The additive systematic uncertainties involve contributions from the

(i) Signal PDF shapes: We characterize them by varying the PDF shape parameters (signal mean, signal width, and combinatorial background shape and normalization) by the statistical uncertainties obtained in the fits to the J/ψ data control samples for m_{ES} and signal MC events for $m_{K\pi}$.

(ii) Hadronic backgrounds: We characterize them by varying both the normalization by the associated statistical uncertainties and by performing fits with different choices of smoothing parameters for the KEYS PDF shapes.

(iii) Peaking backgrounds from charmonium events and π^0/η Dalitz decays: We vary the normalization for these contributions by ±25%.

(iv) Modeling of $m_{K\pi}$ line shapes of the combinatorial background: We characterize the uncertainties by analyzing data samples selected from the $m_{ES} <$ 5.27 GeV/c^2 sideband, and simulated events.

Table IV summarizes all sources of systematic uncertainties considered in the total branching fraction measurements for individual modes. The total systematic uncertainty for the branching fractions is obtained by summing in quadrature the above-described uncertainties from different categories.
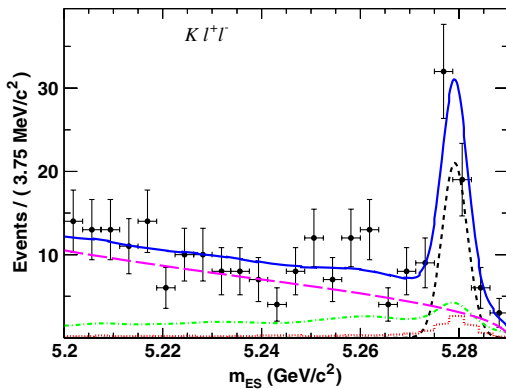

FIG. 5 (color online).   The m_{ES} spectrum in bin s_4 for all $K\ell^+\ell^-$ modes combined showing data (points with error bars), the total fit (blue solid line), signal component (black short-dashed line), combinatorial background (magenta long-dashed line), hadrons misidentified as muons (green dash-dotted line), and the sum of cross-feed and peaking components (red dotted line).
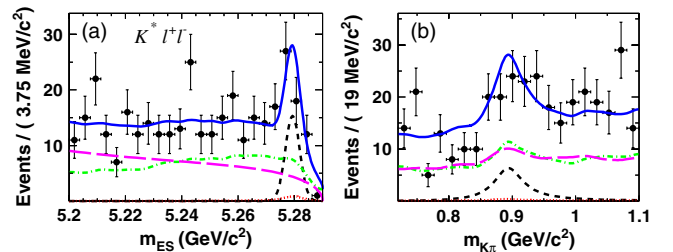

FIG. 6 (color online).   The (a) m_{ES} and (b) $m_{K\pi}$ mass spectra in bin s_1 for all four $K^*\ell^+\ell^-$ modes combined showing data (points with error bars), the total fit (blue solid lines), signal component (black short-dashed lines), combinatorial background (magenta long-dashed lines), hadrons misidentified as muons (green dash-dotted lines), and the sum of cross-feed and peaking components (red dotted lines).

TABLE V. Measured branching fractions [10^{-7}] by mode and s bin. The first and second uncertainties are statistical and systematic, respectively.

	$B \to K\ell^+\ell^-$		$B \to K^*\ell^+\ell^-$	
s (GeV^2/c^4)	N_{sig}	$\mathcal{B}[10^{-7}]$	N_{sig}	$\mathcal{B}[10^{-7}]$
0.10–2.00	$20.6^{+5.9}_{-5.4}$	$0.71^{+0.20}_{-0.18} \pm 0.02$	$26.0^{+7.1}_{-6.4}$	$1.89^{+0.52}_{-0.46} \pm 0.06$
2.00–4.30	$17.4^{+5.4}_{-4.8}$	$0.49^{+0.15}_{-0.13} \pm 0.01$	$14.5^{+5.3}_{-4.6}$	$0.95^{+0.35}_{-0.30} \pm 0.04$
4.30–8.12	$37.1^{+8.0}_{-7.5}$	$0.94^{+0.20}_{-0.19} \pm 0.02$	$29.3^{+9.1}_{-8.3}$	$1.82^{+0.56}_{-0.52} \pm 0.09$
10.11–12.89	$36.0^{+8.2}_{-7.6}$	$0.90^{+0.20}_{-0.19} \pm 0.04$	$31.6^{+8.8}_{-8.1}$	$1.86^{+0.52}_{-0.48} \pm 0.10$
14.21–16.00	$19.7^{+6.2}_{-5.6}$	$0.49^{+0.15}_{-0.14} \pm 0.02$	$24.1^{+6.7}_{-6.0}$	$1.46^{+0.41}_{-0.36} \pm 0.06$
>16.00	$22.3^{+7.7}_{-6.9}$	$0.67^{+0.23}_{-0.21} \pm 0.05$	$14.1^{+6.6}_{-5.9}$	$1.02^{+0.47}_{-0.42} \pm 0.06$
1.00–6.00	$39.4^{+7.7}_{-7.1}$	$1.36^{+0.27}_{-0.24} \pm 0.03$	$33.1^{+8.6}_{-7.8}$	$2.05^{+0.53}_{-0.48} \pm 0.07$

B. Systematic uncertainties for the rate asymmetries

For $\mathcal{A}_{CP}$, a large portion of the uncertainties associated with the signal efficiency cancel. We find that the only efficiency-related term discussed in Sec. VIII A that is not negligible for $\mathcal{A}_{CP}$ is the one associated with the PID selection. Among the efficiency-related systematics, we therefore only consider this term. We also consider the additive systematic uncertainties listed in Sec. VIII A. Our measured $\mathcal{A}_{CP}$ central values for $J/\psi K$ and $J/\psi K^*$ are both well below 1% and show minimal detector efficiency effects. Potential, additional $\mathcal{A}_{CP}$ systematic

effects from the assumptions of lepton-flavor and isospin symmetry are tested by removing these assumptions.

The systematic uncertainties for the lepton-flavor ratios $\mathcal{R}_{K^{(*)}}$ are calculated by summing in quadrature the systematic errors in the muon and electron modes. Common systematic effects, such as tracking, K_S^0 efficiency, and $B\bar{B}$ counting, yield negligible uncertainties in the ratios. Potential, additional $\mathcal{R}_{K^{(*)}}$ systematic effects are tested by removing the assumption of isospin symmetry.

For the systematic uncertainties of $\mathcal{A}_I$, we sum in quadrature the systematic errors in charged and neutral B modes. Common systematic effects, which include $B\bar{B}$ counting and a large portion of the uncertainties associated with PID and tracking efficiencies, are negligible. Again, additional tests on $\mathcal{A}_I$ systematics are performed by relaxing the assumption of lepton-flavor symmetry. Furthermore, as the cross-feed fractions in Tables II and III are estimated under the assumption of isospin symmetry, we test this systematic effect using cross-feed fractions estimated with different $\mathcal{A}_I$ input values.

Our checks on symmetry assumptions described above for $\mathcal{A}_{CP}$, $\mathcal{R}_{K^{(*)}}$ and $\mathcal{A}_I$ generally show deviations from the original measured values below 20% of the associated
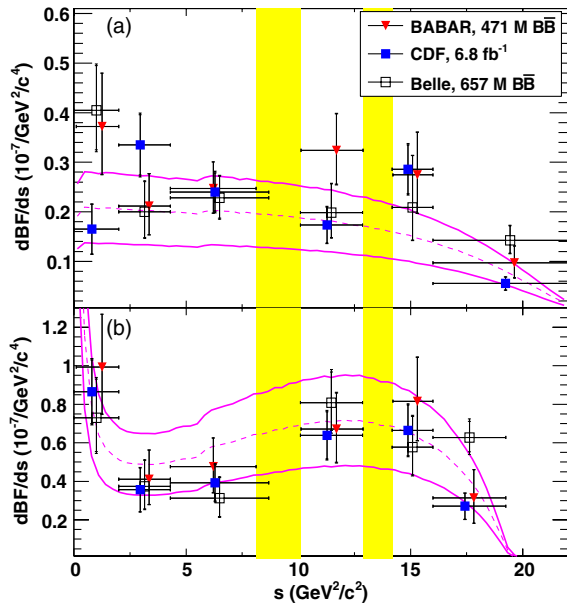

FIG. 7 (color online). Partial branching fractions for the (a) $K\ell^+\ell^-$ and (b) $K^*\ell^+\ell^-$ modes as a function of s showing *BABAR* measurements (red triangles), Belle measurements [27] (open squares), CDF measurements [28] (blue solid squares), and the SM prediction from the Ali *et al.* model [5] with $B \to K^{(*)}$ form factors [31] (magenta dashed lines). The magenta solid lines show the theory uncertainties. The vertical yellow shaded bands show the vetoed s regions around the J/ψ and $\psi(2S)$.
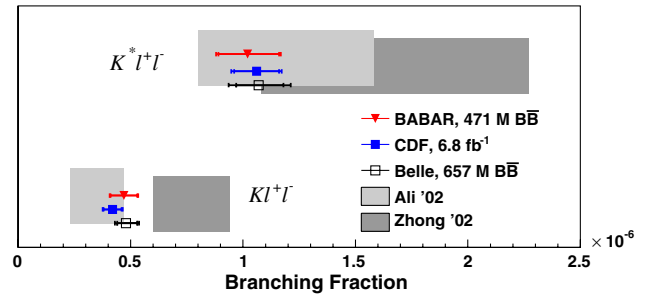

FIG. 8 (color online). Total branching fractions for the $K\ell^+\ell^-$ and $K^*\ell^+\ell^-$ modes (red triangles) compared with Belle [27] (open squares) and CDF [28] (blue solid squares) measurements and with predictions from the Ali *et al.* [5] (light gray bands), and Zhong, Wu, and Wang [6] (dark gray bands) models.
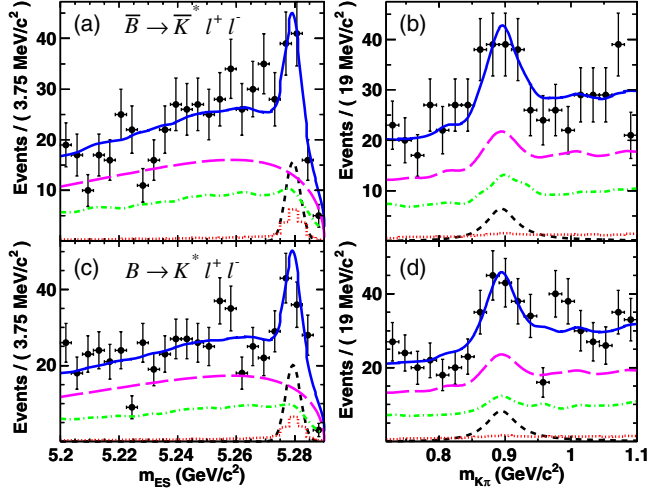
FIG. 9 (color online). (a),(c) m_{ES} and (b),(d) $m_{K\pi}$ fits for $\mathcal{A}_{CP}$ in the (a),(b) $\bar{B}$ and (c),(d) B low s region for all four $K^*\ell^+\ell^-$ modes combined. Data (points with error bars) are shown together with total fit (blue solid lines), combinatorial background (magenta long-dashed lines), signal (black short-dashed lines), hadronic background (green dash-dotted lines), and the sum of cross-feed and peaking background (red dotted lines).

statistical uncertainties, and so we do not assign additional uncertainties.

IX. RESULTS

We perform fits for each $K^{(*)}\ell^+\ell^-$ final state in each s bin listed in Tables II and III to obtain signal and background yields, N_{sig} and N_{bkg}, respectively. We model the different background components by the PDFs described in Sec. VI. We allow the shape parameter of the m_{ES} kinematic threshold function of the combinatorial background to float in the fits. For the signal, we use a fixed Gaussian shape unique to each final state, as described previously. We leave the shapes of the other background PDFs fixed. For the peaking background, we fix the absolute normalization. For the cross feed, we fix the normalization relative to the signal yields.

Figure 5 shows as an example the m_{ES} distribution for the combined $K\ell^+\ell^-$ modes in bin s_4, while Fig. 6 shows the m_{ES} and $m_{K\pi}$ mass spectra for the combined $K^*\ell^+\ell^-$ modes in bin s_1. The cross-feed contributions and the peaking backgrounds are negligible for this fit. The

TABLE VI. Measured $\mathcal{A}_{CP}$ by mode and s region. The first and second uncertainties are statistical and systematic, respectively. "All" refers to the union of $0.10 < s < 8.12$ GeV^2/c^4 and $s > 10.11$ GeV^2/c^4.

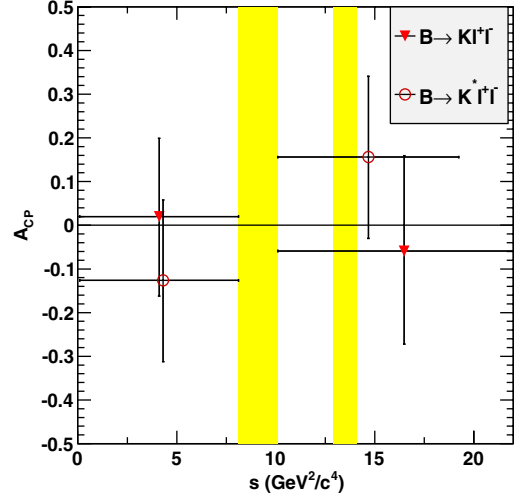| s (GeV^2/c^4)	$A_{CP}(B^+ \to K^+\ell^+\ell^-)$	$A_{CP}(B \to K^*\ell^+\ell^-)$
All	$-0.03 \pm 0.14 \pm 0.01$	$0.03 \pm 0.13 \pm 0.01$
0.10–8.12	$0.02 \pm 0.18 \pm 0.01$	$-0.13^{+0.18}_{-0.19} \pm 0.01$
>10.11	$-0.06^{+0.22}_{-0.21} \pm 0.01$	$0.16^{+0.18}_{-0.19} \pm 0.01$

FIG. 10 (color online). *CP* asymmetries $\mathcal{A}_{CP}$ for $K\ell^+\ell^-$ modes (red solid triangles) and $K^*\ell^+\ell^-$ modes (red open circles) as a function of s. The vertical yellow shaded bands show the vetoed s regions around the J/ψ and $\psi(2S)$.

combinatorial background dominates and for $\mu^+\mu^-$ modes misidentified hadrons are the second largest background. From the yields in each s bin we determine the partial branching fractions summarized in Table V. Figure 7 shows our results for the partial branching fractions of the $K\ell^+\ell^-$ and $K^*\ell^+\ell^-$ modes in comparison to results from the Belle and CDF Collaborations [27,28] and to the prediction of the Ali *et al.* model [5]. Our results are seen to agree with those of Belle and CDF. Our results are also in agreement with the most recent partial branching fraction measurements of $B^0 \to K^{*0}\mu^+\mu^-$ from LHCb [29].

The total branching fractions are measured to be

$$\mathcal{B}(B \to K\ell^+\ell^-) = (4.7 \pm 0.6 \pm 0.2) \times 10^{-7},$$
$$\mathcal{B}(B \to K^*\ell^+\ell^-) = (10.2^{+1.4}_{-1.3} \pm 0.5) \times 10^{-7}.$$

Here, the first uncertainties are statistical, and the second are systematic. The total branching fractions are shown in
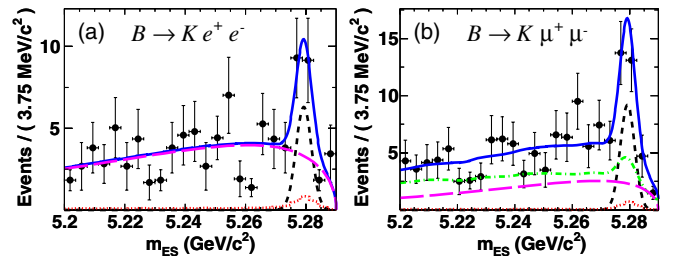

FIG. 11 (color online). m_{ES} fits for $\mathcal{R}_K$ in the (a) Ke^+e^- and (b) $K\mu^+\mu^-$ modes in the high s region. Data (points with error bars) are shown together with total fit (blue solid lines), combinatorial background (magenta long-dashed lines), signal (black short-dashed lines), hadronic background (green dash-dotted lines), and the sum of cross-feed and peaking background (red dotted lines).

TABLE VII. Measured $\mathcal{R}_{K^{(*)}}$ by mode and s region. The first and second uncertainties are statistical and systematic, respectively. All refers to the union of $0.10 < s < 8.12$ GeV$^2/c^4$ and $s > 10.11$ GeV$^2/c^4$.

s (GeV$^2/c^4$)	$\mathcal{R}_K$	R_{K^*}
All	$1.00^{+0.31}_{-0.25} \pm 0.07$	$1.13^{+0.34}_{-0.26} \pm 0.10$
0.10–8.12	$0.74^{+0.40}_{-0.31} \pm 0.06$	$1.06^{+0.48}_{-0.33} \pm 0.08$
>10.11	$1.43^{+0.65}_{-0.44} \pm 0.12$	$1.18^{+0.55}_{-0.37} \pm 0.11$

Fig. 8 in comparison to measurements from Belle [27] and CDF [28] and predictions from Ali *et al.* [5] and Zhong, Wu, and Wang [6].

To measure direct $\mathcal{A}_{CP}$, we fit the B and $\bar{B}$ samples in the two $K^+\ell^+\ell^-$ modes and four $K^*\ell^+\ell^-$ modes listed in Sec. IV. We perform the measurements in the full s region, as well as in the low s and high s regions separately. The B and $\bar{B}$ data sets share the same background shape parameter for the kinematic threshold function. Figure 9 shows an example fit for the combined $B \to K^*\ell^+\ell^-$ modes in the low s region. Table VI summarizes the results. Figure 10 shows $\mathcal{A}_{CP}$ as a function of s. Our results are consistent with the SM expectation of negligible direct $\mathcal{A}_{CP}$.

We fit the e^+e^- and $\mu^+\mu^-$ samples in the four $K\ell^+\ell^-$ modes and four $K^*\ell^+\ell^-$ modes in the low s and high s regions separately to measure the lepton-flavor ratios. Figure 11 shows an example fit for the combined $K\mu^+\mu^-$ and Ke^+e^- modes in the high s region. Table VII and Fig. 12 show $\mathcal{R}_K$ and $\mathcal{R}_{K^*}$ for $s > 0.1$ GeV$^2/c^4$. Our results are consistent with unity as expected in the SM.

We fit the data in each s bin separately to determine $\mathcal{A}_I$ for the four combined $K\ell^+\ell^-$ and four combined $K^*\ell^+\ell^-$
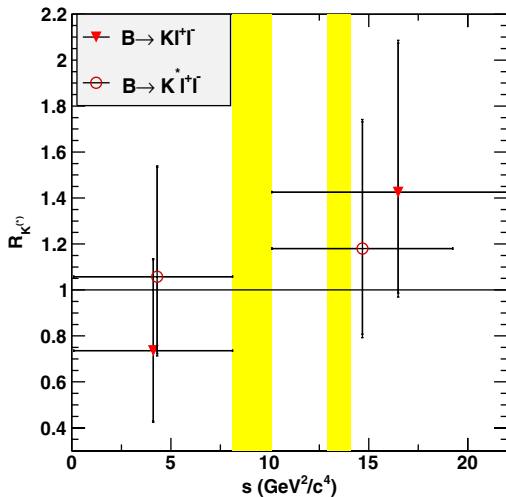

FIG. 12 (color online). Lepton-flavor ratios $\mathcal{R}_{K^{(*)}}$ for the $K\ell^+\ell^-$ (red solid triangles) and $K^*\ell^+\ell^-$ modes (red open circles) as a function of s. The vertical yellow shaded bands show the vetoed s regions around the J/ψ and $\psi(2S)$.
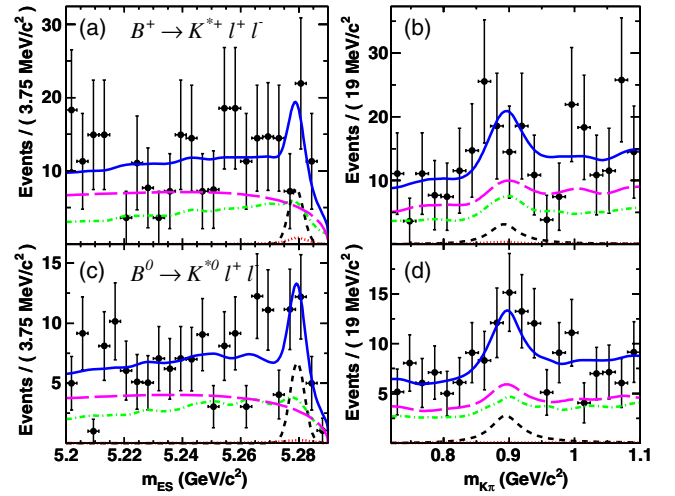

FIG. 13 (color online). The $m_{\rm ES}$ and $m_{K\pi}$ fit projections for the (a),(b) $K^{*+}\ell^+\ell^-$ and (c),(d) $K^{*0}\ell^+\ell^-$ modes in bin s_2. Data (points with error bars) are shown together with total fit (blue solid lines), combinatorial background (magenta long-dashed lines), signal (black short-dashed lines), hadronic background (green dash-dotted lines), and the sum of cross-feed and peaking background (red dotted lines).

modes. Figure 13 shows an example fit for bin s_2. The results are summarized in Table VIII. Figure 14 shows our measurements as a function of s in comparison with those of Belle [27]. The two sets of results are seen to agree within the uncertainties. Our results are also consistent with the SM prediction that $\mathcal{A}_I$ is slightly negative ($\sim -1\%$) except in bin s_1, where it is predicted to have a value around $+5\%$ [4].

Our $\mathcal{A}_I$ measurements in the low s region ($0.10 < s < 8.12$ GeV$^2/c^4$) yield

$$\mathcal{A}_I^{\rm low}(B \to K\ell^+\ell^-) = -0.58^{+0.29}_{-0.37} \pm 0.02[2.1\sigma],$$

$$\mathcal{A}_I^{\rm low}(B \to K^*\ell^+\ell^-) = -0.25^{+0.20}_{-0.17} \pm 0.03[1.2\sigma],$$

where the first uncertainty is statistical and the second is systematic. The $\mathcal{A}_I$ significances shown in the square brackets include all systematic uncertainties. We estimate

TABLE VIII. Measured $\mathcal{A}_I$ by mode and s bin. The first and second uncertainties are statistical and systematic, respectively.

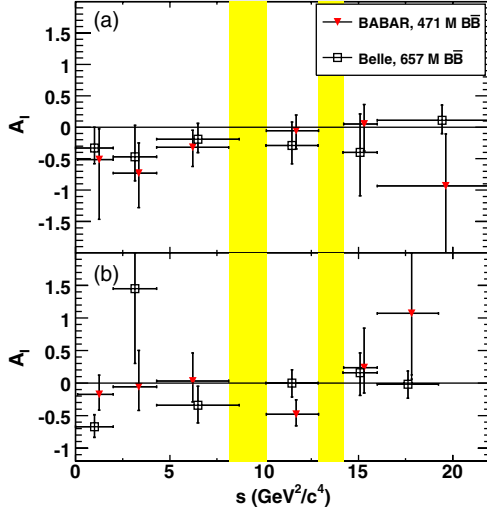|	$\mathcal{A}_I$	
s (GeV$^2/c^4$)	$B \to K\ell^+\ell^-$	$B \to K^*\ell^+\ell^-$
0.10–2.00	$-0.51^{+0.49}_{-0.95} \pm 0.04$	$-0.17^{+0.29}_{-0.24} \pm 0.03$
2.00–4.30	$-0.73^{+0.48}_{-0.55} \pm 0.03$	$-0.06^{+0.56}_{-0.36} \pm 0.05$
4.30–8.12	$-0.32^{+0.27}_{-0.30} \pm 0.01$	$0.03^{+0.43}_{-0.32} \pm 0.04$
10.11–12.89	$-0.05^{+0.25}_{-0.29} \pm 0.03$	$-0.48^{+0.22}_{-0.18} \pm 0.05$
14.21–16.00	$0.05^{+0.31}_{-0.43} \pm 0.03$	$0.24^{+0.61}_{-0.39} \pm 0.04$
>16.00	$-0.93^{+0.83}_{-4.99} \pm 0.04$	$1.07^{+4.27}_{-0.95} \pm 0.35$
1.00–6.00	$-0.41 \pm 0.25 \pm 0.01$	$-0.20^{+0.30}_{-0.23} \pm 0.03$

FIG. 14 (color online). Isospin asymmetry $\mathcal{A}_I$ for the (a) $K\ell^+\ell^-$ and (b) $K^*\ell^+\ell^-$ modes as a function of s (red triangles), in comparison to results from Belle [27] (open squares). The vertical yellow shaded bands show the vetoed s regions around the J/ψ and $\psi(2S)$.

the significance by refitting the data with $\mathcal{A}_I$ fixed to zero and compute the change in log likelihood $\sqrt{2\Delta \ln \mathcal{L}}$ between the nominal fit and the null hypothesis fit.

X. CONCLUSION

In summary, we have measured total and partial branching fractions, direct CP asymmetries, lepton-flavor ratios, and isospin asymmetries in the rare decays $B \to K^{(*)}\ell^+\ell^-$ using 471×10^6 $B\bar{B}$ pairs. These results provide an update to our previous measurements on branching fractions and rate asymmetries excluding the $s < 0.1$ GeV$^2/c^4$ region [30]. The total branching fractions, $\mathcal{B}(B \to K\ell^+\ell^-) = (4.7 \pm 0.6 \pm 0.2) \times 10^{-7}$ and $\mathcal{B}(B \to K^*\ell^+\ell^-) = (10.2^{+1.4}_{-1.3} \pm 0.5) \times 10^{-7}$, are measured with precisions of 13% and 14%, respectively. The partial branching fractions as a function of s agree

well with the SM prediction. For $0.10 < s < 8.12$ GeV$^2/c^4$, our partial branching fraction results also allow comparisons with soft-collinear effective theory based predictions. CP asymmetries for both $B \to K\ell^+\ell^-$ and $B \to K^*\ell^+\ell^-$ are consistent with zero and the lepton-flavor ratios are consistent with one, both as expected in the SM. The isospin asymmetries at low s values are negative. For $0.10 < s < 8.12$ GeV$^2/c^4$ we measure $\mathcal{A}_I(B \to K\ell^+\ell^-) = -0.58^{+0.29}_{-0.37} \pm 0.02$ and $\mathcal{A}_I(B \to K^*\ell^+\ell^-) = -0.25^{+0.20}_{-0.17} \pm 0.03$. The isospin asymmetries are all consistent with the SM predictions. All results are in good agreement with those of the Belle, CDF, and LHCb experiments.

[1] G. Buchalla, A. J. Buras, and M. E. Lautenbacher, Rev. Mod. Phys. **68,** 1125 (1996).

[2] W. Altmannshofer, P. Ball, A. Bharucha, A. J. Buras, D. M. Straub, and M. Wick, J. High Energy Phys. 01 (2009) 019.

[3] G. Burdman, Phys. Rev. D **52,** 6400 (1995); J. L. Hewett and J. D. Wells, Phys. Rev. D **55,** 5549 (1997); Y. G. Xu, R. M. Wang, and Y. D. Yang, Phys. Rev. D **74,** 114019 (2006); P. Colangelo, F. De Fazio, R. Ferrandes, and T. N. Pham, Phys. Rev. D **73,** 115006 (2006).

[4] T. Feldmann and J. Matias, J. High Energy Phys. 01 (2003) 074.

[5] A. Ali, E. Lunghi, C. Greub, and G. Hiller, Phys. Rev. D **66,** 034002 (2002).

[6] M. Zhong, Y.-L. Wu, and W.-Y. Wang, Int. J. Mod. Phys. A **18,** 1959 (2003).

[7] A. Ali, P. Ball, L. T. Handoko, and G. Hiller, Phys. Rev. D **61,** 074024 (2000); M. Beneke, T. Feldmann, and D. Seidel, Nucl. Phys. **B612,** 25 (2001); W. Altmannshofer, P. Ball, A. Bharucha, A. J. Buras, D. M. Straub, and M. Wick, J. High Energy Phys. 01 (2009) 019; C. Bobeth, G. Hiller, and D. van Dyk, J. High Energy Phys. 07 (2010) 098; A. Khodjamirian, T. Mannel, A. A. Pivovarov, and Y.-M. Wang, J. High Energy Phys. 09 (2010) 089.

[8] A. K. Alok, A. Datta, A. Dighe, M. Duraisamy, D. Ghosh, D. London, and S. U. Sankar, J. High Energy Phys. 11 (2011) 121; A. K. Alok, A. Datta, A. Dighe, M. Duraisamy, D. Ghosh, and D. London, J. High Energy Phys. 11 (2011) 122.

[9] Q.-S. Yan, C.-S. Huang, W. Liao, and S.-H. Zhu, Phys. Rev. D **62**, 094023 (2000).

[10] A. Ali, G. Kramer, and G.-H. Zhu, Eur. Phys. J. C **47**, 625 (2006).

[11] Charge conjugation is implied throughout except as explicitly noted.

[12] F. Kruger, L. M. Sehgal, N. Sinha, and R. Sinha, Phys. Rev. D **61**, 114028 (2000); **63**, 019901(E) (2001).

[13] G. Hiller and F. Kruger, Phys. Rev. D **69**, 074020 (2004).

[14] K. Nakamura *et al.* (Particle Data Group), J. Phys. G **37**, 075021 (2010).

[15] B. Aubert *et al.* (*BABAR* Collaboration), Phys. Rev. D **70**, 112006 (2004).

[16] M. Beneke, T. Feldmann, and D. Seidel, Eur. Phys. J. C **41**, 173 (2005).

[17] T. Feldmann, in Proceedings of the Fifth Workshop on the CKM Unitary Triangle, Rome, 2008 (unpublished).

[18] B. Aubert *et al.* (*BABAR* Collaboration), Nucl. Instrum. Methods Phys. Res., Sect. A **479**, 1 (2002).

[19] L. Breiman, Mach. Learn. **24**, 123 (1996); I. Narsky, arXiv:physics/0507157.

[20] G. C. Fox and S. Wolfram, Phys. Rev. Lett. **41**, 1581 (1978).

[21] B. Aubert *et al.* (*BABAR* Collaboration), Phys. Rev. Lett. **89**, 281802 (2002).

[22] B. Aubert *et al.* (*BABAR* Collaboration), Phys. Rev. D **78**, 071103 (2008).

[23] H. Albrecht *et al.* (ARGUS Collaboration), Z. Phys. C **48**, 543 (1990).

[24] K. S. Cranmer, Comput. Phys. Commun. **136**, 198 (2001).

[25] B. Aubert *et al.* (*BABAR* Collaboration), Phys. Rev. D **73**, 092001 (2006).

[26] T. Allmendinger *et al.*, arXiv:1207.2849.

[27] J.-T. Wei *et al.* (BELLE Collaboration), Phys. Rev. Lett. **103**, 171801 (2009).

[28] T. Aaltonen *et al.* (CDF Collaboration), Phys. Rev. Lett. **107**, 201802 (2011).

[29] R. Aaij *et al.* (LHCb Collaboration), Phys. Rev. Lett. **108**, 181806 (2012)

[30] B. Aubert *et al.* (*BABAR* Collaboration), Phys. Rev. Lett. **102**, 091803 (2009).

[31] P. Ball and R. Zwicky, Phys. Rev. D **71**, 014015 (2005); **71**, 014029 (2005).